Enigmatic tsunami waves amplified by repetitive source events near Sofugan volcano, Japan

Osamu Sandanbata[1†], Kenji Satake[1], Shunsuke Takemura[1], Shingo Watada[1], Takuto Maeda[2], and Tatsuya Kubota[3]

[1]Earthquake Research Institute, The University of Tokyo, Tokyo, Japan.

[2]Graduate School of Science and Technology, Hirosaki University, Aomori, Japan.

[3]National Research Institute for Earth Science and Disaster Resilience, Ibaraki, Japan.

Corresponding author: Osamu Sandanbata (osm3@eri.u-tokyo.ac.jp)

Key Points

- On 8 October 2023 (UTC), enigmatic tsunamis up to ~60 cm were recorded along broad Japanese coasts without large earthquakes.
- Analysis of stacked tsunami waveform data shows >10 events intermittently caused tsunamis for ~1.5 hr with T-phase and seismic excitation.
- Larger events later in the sequence occurred with intervals similar to the wave period, amplifying the tsunami waves in the later phase.

Plain Language Summary

On 8 October 2023, mysterious tsunamis hit Izu Islands and southwestern Japan, reaching up to 60 cm in height, although only small-to-moderate seismic events were reported in the region. To resolve how the mysterious tsunami waves were generated, we analyze the waves recorded by a tsunami observation network off the southwestern coast of Japan. We find that the tsunami waves were intermittently produced by repetitive source events for approximately 1.5 hours, and the wave amplification happened because the inter-event times matched the wave periods. These abnormal submarine events excited significant acoustic oceanic waves, as well as measurable tsunamis, which provides valuable information to further study what took place in the ocean.

Abstract

On 8 October 2023, mysterious tsunamis with a maximum wave height of 60 cm were observed in Izu Islands and southwestern Japan, although only seismic events with body-wave magnitudes m_b 4–5 have been documented to the west of Sofugan volcano. To investigate the source process, we analyze tsunami waveforms recorded by an array network of ocean bottom pressure gauges. A stacked waveform of pressure gauge records suggests recurrent arrivals of multiple wave trains. Deconvolution of the stacked waveform by a tsunami waveform from an earlier event revealed over 10 source events that intermittently generated tsunamis for ~1.5 hours. The temporal history of this sequence corresponds to the origin times of T-phases estimated by an ocean bottom seismometer and of the seismic swarm, implying a common origin. Larger events later in the sequence occurred at intervals comparable to the tsunami wave period, causing amplification of later phases of the tsunami waves.

1 Introduction

On 8 October 2023 (UTC), enigmatic tsunamis were observed along coasts in broad region from south to west of Japan. The tsunami heights, measured from zero to crest, were 30–60 cm in Izu Islands (Yaene, Tsubota, and Kozushima) and the Kanto region (Mera), and 30–40 cm tsunamis were recorded even in distant stations (Tosashimizu and Nakanoshima) (Japan Meteorological Agency, 2023) (Figure 1a). Because no significant earthquake was observed and no offshore tsunami observation system is deployed off Izu-Bonin Islands, the tsunami forecasting system did not work well; it was only after the tsunami started to be recorded clearly by a tsunami-meter at Yaene on Hachijojima Island that the tsunami advisory was issued by Japane Meterological Agency (JMA).

From 18:58 to 21:26 (UTC) on the day, 15 seismic events with body-wave magnitudes m_b 4.3–5.4 took place in the oceanic region approximately 20–30 km to the west of Sofugan volcano (Japan Meteorological Agency, 2013; Global Volcanism Program, 2023), an emergent portion of the submarine volcano, according to the earthquake catalog of U. S. Geological Survey (USGS; Figure 1c); these seismic events are labelled as *Se01–15* (Table S1). The amplitudes of the observed tsunamis were much larger than those expected from the seismic magnitudes; the tsunami magnitude based on the maximum amplitude information at coastal tide gauges reported by JMA is estimated as M_t 8.0 (Abe, 1981), suggesting its atypical source mechanism. For such tsunamis without large earthquakes, various mechanisms have been proposed: slow-ruptured tsunami earthquakes along subduction zones (e.g., the 1896 Sanriku earthquake, the 1946 Aleutian earthquake) (Kanamori, 1972; Tanioka & Satake, 1996), oceanic volcanic processes (e.g., the 2018 Anak Krakatau eruption, the 2022 Hunga Tonga–Hunga

Ha‘apai eruption) (Kubota et al., 2022; Mulia et al., 2020; Paris, 2015), or submarine/coastal landslides or mass failures (e.g., the 1998 Papua New Guinea tsunami) (Synolakis et al., 2002; Tappin et al., 1999).

This study investigates the source process of the enigmatic tsunami waves using tsunami waveform data of spatially dense ocean bottom pressure (OBP) gauges off the southwestern coast of Japan. We first apply a waveform stacking technique to the multiple tsunami waveforms, and then estimate the temporal history of the tsunami generation based on the analysis of the stacked data. Consequently, we propose their peculiar tsunami origin by repetitive source events that took place intermittently for ~1.5 hours.

2 Data

The tsunami waves were recorded by the OBP gauges of Dense Oceanfloor Network system for Earthquakes and Tsunamis (DONET) off the southwestern coast of Japan (Figure 1b) (National Research Institute for Earth Science and Disaster Resilience, 2019). In Figure 2a, we show the OBP data after removing the tidal component, demonstrating repetitive strong high-frequency (>1 Hz) signals approximately from 19:00 to 21:30 (see Figure S1). These high-frequency signals are T-phases, seismic waves converted from oceanic acoustic waves (Okal, 2008), based on their arrival times explained by a typical T-phase speed of 1.5 km/s from the origin times and locations of the seismic events. Following the T-phase signals, tsunami waves with longer periods were recorded, as shown evidently in the band-pass (0.00125–0.02 Hz/50–800 s) filtered records (Figure 2b). Smaller oscillations start around 20:40, leading to the largest amplitudes of ~20 mm after ~22:00, exhibiting long-lasting tsunamis for hours with late arrivals of the largest waves.

To capture the features, a tsunami waveform stacking technique is applied to two sets of >10 OBP records of nearby stations: (1) 16 records of DONET1 (KMA–KME), and (2) 13 records of DONET2 (MRC–MRE) (Table S2). By assuming a point source near the source region of the seismic event swarm on 8 October 2023 (140.026°E, 29.787°N), the tsunami travel times to the stations are computed by a shallow-water-wave tsunami model of the Geoware TTT Software (Figure S2). The band-pass filtered OBP waveform at each station is shifted as the arrival times are aligned with that at the earliest-arrival station (KMC21 for DONET1, and MRE20 for DONET2). We then stack the time-shifted waveforms and take the amplitude average and the standard deviation.

We show the stacked waveform of DONET1 in Main Text (Figures 2c–e) and contain that of DONET2 in Supporting Information (Figure S3). As shown in Figures 2c and 2d, all the DONET1 waveforms here show similar shapes; thereby, the waveform stacking yields clear tsunami waveforms only with small standard deviations. The tsunami waves initiate at ~120 min (~20:40) and reach the maximum amplitude at ~220 min (~22:10).

For further investigation, we apply the wavelet analysis to the stacked waveform (Figure 2e). The obtained scalogram shows that the tsunami signals are composed of multiple bends of dispersive amplitude peaks with early arrival of lower-frequency amplitude followed by higher-frequency amplitude (red arrows and a bracket in Figure 2e). The same feature can be seen in the stacked waveform of DONET2 (Figure S3). This feature with multiple bands is quite different from a tsunami event originating from a single volcanic earthquake at Sumisu Caldera, which exhibits only a single band (Figure S4; see the caption for details). Therefore, we speculate that multiple tsunami wave trains, each with a strongly dispersive character, recurrently arrived at the OBP gauges.

3 Estimation of source time function

Using the stacked tsunami waveforms obtained above, we investigate the temporal history of the tsunami generation process using the iterative deconvolution method, which has been widely applied in earthquake source studies. We separately analyze the two stacked waveforms of DONET1 and DONET2 in the same way, but the methodology is explained below with the waveform of DONET1.

We hypothesize that multiple source events took place at the same location but at different timings, and that each single event produced tsunami waveforms with the same shapes and different amplitudes. Under this hypothesis, the stacked OBP tsunami waveform is the convolution of the temporal history of multiple source events, or the *tsunami source time function* (STF), and the tsunami waveform produced by a single event, or the *Green's function*. Denoting the stacked tsunami waveform as $d(t)$ and the Green's function as $w(t)$, the convolution can be expressed, as follows:

$$d(t) = \sum_i m_i w(t - t_i), \qquad (1)$$

where m_i and t_i represent the source amplitude and timing of the i-th iteratively determined source event, respectively, as explained in detail later.

The Green's function is extracted from the stacked tsunami waveform data; in other words, we prepare an empirical Green's function (e.g., Wang et al., 2022). We first confirm that the first seismic event Se01 did not produce measurable tsunami waves, but that the theoretical arrival times of the tsunamis caused by Se02 and Se03, agree well with the timings when the tsunami signal initiates (~20:40) and when the amplitude increases (~21:00), respectively (arrows in Figure 3a). We assume that the signal between the two tsunami arrival times represent

the tsunami waveform due to Se02, and construct the Green's function by adding an initial zero-amplitude data for the length of the theoretical tsunami travel time to the stacked waveform in the time window (with tapering on the 5% edges) (green line in Figure 3a). m_i in Equation (1) now represents the relative source amplitude of the *i*-th source event to that of Se02, and we impose $m_i \geq 0$ under our hypothesis of multiple similar events.

Using the Green's function, we deconvolve the stacked tsunami waveform (Figure 3a) to estimate the tsunami STF, following Kikuchi and Kanamori (1982). Denoting the stacked tsunami waveform as $x(t)$, we first take a single event and determine m_1 and t_1 by minimizing the error defined as

$$\Delta_1 = \int_0^T [x(t) - m_1 w(t - t_1)]^2 dt, \qquad (2)$$

where T is the length of the stacked waveform ($t = 0$ at 18:30, and $t = T$ at 23:30), and obtain the residual waveform $x^{(1)}(t)$:

$$x^{(1)}(t) = x(t) - m_1 w(t - t_1). \qquad (3)$$

In the *i*-th iteration, m_i and t_i are determined by minimizing the error Δ_i,

$$\Delta_i = \int_0^T \left[x^{(i-1)}(t) - m_i w(t - t_i)\right]^2 dt, \qquad (4)$$

which yields the residual waveform $x^{(i)}(t)$:

$$x^{(i)}(t) = x^{(i-1)}(t) - m_i w(t - t_i). \qquad (5)$$

We iteratively repeat the procedure above until the approximation error changes by less than 2% by an iteration ($(\Delta_{i-1} - \Delta_i)/\Delta_{i-1} < 0.02$). The approximation accuracy is quantified by the normalized approximation error:

$$\Delta_i/\Delta_0 = \int_0^T \left[x^i(t)\right]^2 dt \,/\, \int_0^T [x(t)]^2 dt. \qquad (6)$$

Thus, we determine the relative source amplitudes of m_i at the timings of t_i ($i = 1, \ldots N$).

We find that, in the iterative deconvolution process, the source amplitudes determined in earlier iterations tend to be larger, because the original observed waveform is fit mainly by earlier-determined events, and later events are fit to the residual waveforms (Kikuchi & Kanamori, 1982). As seen in the iterative deconvolution results (Figure S5), a source event at 21:17, determined in the first iteration, has a very large source amplitude. To examine how reliable the results are, we re-determine the source amplitudes by an additional least-squares method. While fixing the source event times t_i, we re-estimate the source amplitude m_i' by minimizing the following error, $x(t) - \sum_{i=1}^{N} m_i' w(t - t_i)$, by the non-negative least-squares method (Lawson & Hanson, 1974). Thus, we obtain the tsunami STF, represented by the relative source amplitude m_i' at the source times of t_i. The tsunami waveform is modeled with Equation (1), where m_i is replaced by m_i'. The additional least-squares method improves the amplitude balance of several source events close in time, determines the amplitude of an event as zero, which we remove from the event list; then, the normalized approximation error is reduced significantly from 0.174 to 0.118 (compare Figure S5 with Figure 3).

4 Results

As main results, we show the tsunami STF based on the analysis of the stacked waveform of DONET1 (Figure 3). The tsunami STF is composed of 23 source events that span from 19:53 to 22:02, labeled as *Ts01–23* (Figure 3c and Table S3). The fit between the stacked waveform and the convolved waveform is remarkably good (Figure 3b). This supports our hypothesis that

repetitive tsunami source events took place at similar locations, intermittently producing similar tsunami waveforms.

Since our empirical Green's function contains about five wave cycles but excludes later waves, such as slowly propagating higher-frequency waves and reflected waves on coasts, this may cause artifacts in our estimation due to overfitting to unmodelled later waves from preceding events. Later events, such as Ts17–23, may be less reliable because the later waves from the large-amplitude preceding events (e.g., Ts13, 14 and 15) can cause nonnegligible artifacts. In Figure S6, we demonstrate that most parts of the stacked waveform can be well constructed by the events up to Ts16. For a similar reason, some events that are close to each other with a time difference of only <~100 s (Ts06–07, and Ts09–10) may be separately deconvolved from a single event.

Given the imperfect Green's function, we here consider major source events took place at the timings of Ts01–05, 07–09, and 11–16, which spans from 19:53 (Ts01) to 21:26 (Ts16) for over 1.5 hours (Figure 3c). The sequence of the major events gradually increases the relative source amplitude from 1.0 to 6.5 and reduces the interval time approximately from 1,200 s to 250 s (Table S3).

The later major events with larger amplitudes (e.g., Ts11–16) occur with inter-event times of 200–300 s (Figure 3c, and Table S3), which are comparable to the dominant period of the observed tsunami waveforms (Figure 2e). Figure 4a shows tsunami waveforms from Ts11–16, each of which has a non-negligible amplitude of ~10 mm, still less than half of the amplitude of the stacked largest waves. Yet, their waveform phases match with each other, and thereby the superposition of the tsunami waveforms doubles the wave amplitude and reproduces the largest waves (Figure 4b). Therefore, the late arrivals of the largest tsunami waves can be attributed to

the later large events with inter-event times similar to the characteristic period of the tsunami waves.

The major events in the tsunami STF correlate well with the swarm of seismic events reported in the USGS catalog. In Figure 3d, we compare the tsunami STF with the seismic events Se01–15 (Table S1). Each of Se02–15, excluding Se01, nearly coincides with one of the major tsunami source events up to Ts16, and the overall trends in event size are also similar.

We also investigate origins of the T-phase signals by analyzing the vertical component of a broadband ocean bottom seismometer (OBS) at KMB06 (Figure 1b); we apply the band-pass (1–6Hz) filter, convert the waveform into envelope by the Hilbert transform and the moving average with a 5-s window, and identify T-phase signals with a maximum amplitude larger than an empirical threshold of 2.0×10^3 nm/s. The origin times of the signals are estimated by shifting the maximum amplitude time backward by the T-phase travel time from a seismic source location (140.026°E, 29.787°N) to KMB06 (5.48 min). As results, we detect 14 T-phase events, labeled as *Tp01–14* (Figure 3d and Table S4). The temporal history of the T-phase events, except for Tp01, agrees with the tsunami STF (Figure 3c), as well as the seismic event swarm (Figure 3d), in terms of the origin times and the overall trend in size.

In Supporting Information, we show the results using the stacked tsunami waveform obtained with the 13 records of DONET2 (Figure S7). The estimated tsunami STF contains source events corresponding to the major events determined by the analysis of DONET1, exhibiting similar trends in size and inter-event time and the coincidence with the seismic and T-phase origin times.

5 Discussion & Conclusions

Table S5 summarizes 15 source events (labeled as *EV01–15*), which have similar origin times based on data of tsunami waves, seismic waves, and/or T-phases. The event EV01 at 18:58, detected as seismic and T-phase events (Se01 and Tp01), did not generate measurable tsunami waves. EV02–14, from 19:53 to 21:21, are all detected as tsunami, seismic and T-phase sources. EV15 at 21:26, listed as seismic and tsunami sources, did not excite a T-phase signal strong enough to be identified based on our detection, but its T-phase signal can be seen as a small peak in the OBS record (around Se15 in Figure 3d).

Thus, we suggest that the 14 repetitive events (EV02–15) excited strong T-phases and notable tsunami waves, with seismic radiation equivalent to m_b 4–5. Although the mechanism of the repetitive events remains to be solved, the coincidental excitation of T-phases and tsunamis implies a very shallow source depth in the crust or just on the seafloor. T-phase data may constrain the water depth where the events took place, considering the efficient excitation in a water depth of ~1,000 m, a range of the so-called SOFAR channel (Okal, 2008). On the other hand, the tsunamigenesis requires a large volume of displaced seawater by such as seafloor deformation or mass movement on the seafloor.

Several possible candidates satisfying these conditions remain. Volcanic processes in the ocean, ranging from eruptions (Purkis et al., 2023; Yamasato et al., 1993), flank failures (Grilli et al., 2019), intra-caldera faulting (Sandanbata et al., 2023), and caldera collapse (Maeno et al., 2006) may explain these characters. Submarine landslides or mass failures can be also possible, as T-phases were recorded around the timing of the 1998 Papua New Guinea tsunami (Okal, 2003).

Prompt reports have been published that indicate associations of the sequence to submarine volcanic activities. In late October 2023, Japan Coast Guard (2023) found drifted materials in the sea around Torishima and Sofugan volcanoes, parts of which were analyzed and confirmed as volcanic pumices (Earthquake Research Institute, the University of Tokyo, 2023; Geological Survey of Japan, National Institute of Advanced Industrial Science and Technology, 2023). Mizutani & Melgar (2023) analyzed parts of the tsunami waveforms, suggesting its possible origin of submarine volcanic activity. In early November, Japan Agency for Marine-Earth Science and Technology (2023) surveyed the seafloor near the source region and preliminarily reported the existence of a submarine caldera ~20 km to the west of Sofugan volcano. Hence, we speculate the tsunami sequence is associated with volcanic unrest, most likely near the submarine caldera.

Another series of abnormal tsunamis have recurrently taken place, almost every 10 years, due to M_w 5.4–5.8 volcanic earthquakes at another submarine caldera, Sumisu Caldera (Figure 1c) (Kanamori et al., 1993; Satake & Kanamori, 1991), for which a submarine trapdoor faulting in the inflating caldera was proposed (Sandanbata et al., 2022); the same mechanism has been recently proposed for tsunamigenic earthquakes at two other submarine calderas: Curtis Caldera, New Zealand (Sandanbata et al., 2023), and Kita-Ioto Caldera, Japan (Sandanbata & Saito, 2024). These submarine trapdoor faulting are tsunamigenic but exhibit atypically inefficient seismic excitation (Sandanbata et al., 2021; 2022). Repetitive T-phase events possibly related to volcanic activity also followed the event in 1996 (M_w 5.7) at Sumisu Caldera (Sugioka et al., 2000). Considering these past observations, the trapdoor faulting mechanism at the newly found caldera near Sofugan volcano may be a plausible candidate for the October 2023 tsunamis.

However, the mechanisms proposed above cannot be distinguished from our analysis focusing on the temporal history of the tsunami generation. In future studies, it is critical to reveal the exact locations and initial shapes of the repetitive tsunamis, and a compilation of datasets of tsunamis, seismic waves, and T-phases would be the key to understand the relationship between the October 2023 sequence and submarine volcanic activity.

The repetitive character of EV02–15 infers how the series of phenomena proceeded. As seen in Figures 4c and 4d, the source event number increases exponentially with time, and the inter-event interval of the events gradually decreases. Hotovec et al. (2012) reported that the swarm of repeating earthquakes at Redout Volcano, Alaska, accelerated into an explosive eruption, with decreasing inter-event times and increasing event magnitudes. Different geological phenomena with similar characteristics were also reported for landslide events (Yamada et al., 2016), collapse events of volcanic calderas (Michon et al., 2009; T. A. Wang et al., 2023), and fault slip in tectonic environment (Igarashi, 2000).

In contrast to EV02–15, EV01 did not generate measurable tsunami waves but accompanied strong T-phases and detectable seismic waves. The envelope shape of the T-phase of EV01 exhibits slower amplitude increase and longer duration than those of the others (Figure 3d), indicating its different source mechanism or properties. Although we have considered that tsunami source events Ts17–23, after EV15, are less reliable due to the imperfect Green's function, it is also possible that these later sources have generated tsunamis without notable seismic waves or T-phases, since strength of seismic waves and T-phases can significantly change due to differences in source depth and/or location (e.g., Fukao et al., 2018; Wech et al., 2018).

The 8 October 2023 tsunami sequence was preceded by another seismic swarm mainly from 2 to 6 October, including two M_w>6 earthquakes (Figure 1c). The relationship between the two swarms is unclear, but we note that some earthquakes on 5 October radiated much stronger seismic waves than the 8 October sequence, although high-frequency T-phase signals are larger for the latter (compare Figures S1 and S8), indicating a significant difference in their source mechanism or depth. One possible hypothesis for the link is that the preceding swarm was related to the movement of magma in the crust, leading to another phase of tsunamigenic volcanic process, such as volcanic deformation, underwater eruptions, or flank collapses. Another is that ground shaking due to the preceding swarm destabilized parts of sloped bathymetry, leading to mass failures a few days later.

The enigmatic tsunamis on 8 October 2023 sheds light on the difficulty in forecasting tsunamis without any significant earthquake in the Izu-Bonin region, where no offshore tsunami observation system is deployed. The coincidence of strong T-phases with tsunami generation may help estimate the tsunami potential in advance, as has been long suggested (Ewing et al., 1950; Matsumoto et al., 2016). However, the Izu-Bonin region hosts tens of volcano islands and submarine volcanoes, and active back-arc rift systems (Kodaira et al., 2007), implying various types of potential tsunami hazards. As discussed above, M>5 trapdoor faulting earthquakes can cause notable tsunamis from submarine calderas (Sandanbata et al., 2022; Sandanbata & Saito, 2024). An M_w 6.4 normal faulting earthquake on 24 October 2006 in a region between Sofugan volcano and Nichiyo Seamount (Figure 1c) also generated about 10-cm tsunamis (Japan Meteorological Agency, 2023). In this context, there is an urgent need to improve preparedness for tsunami hazards in the oceanic region.

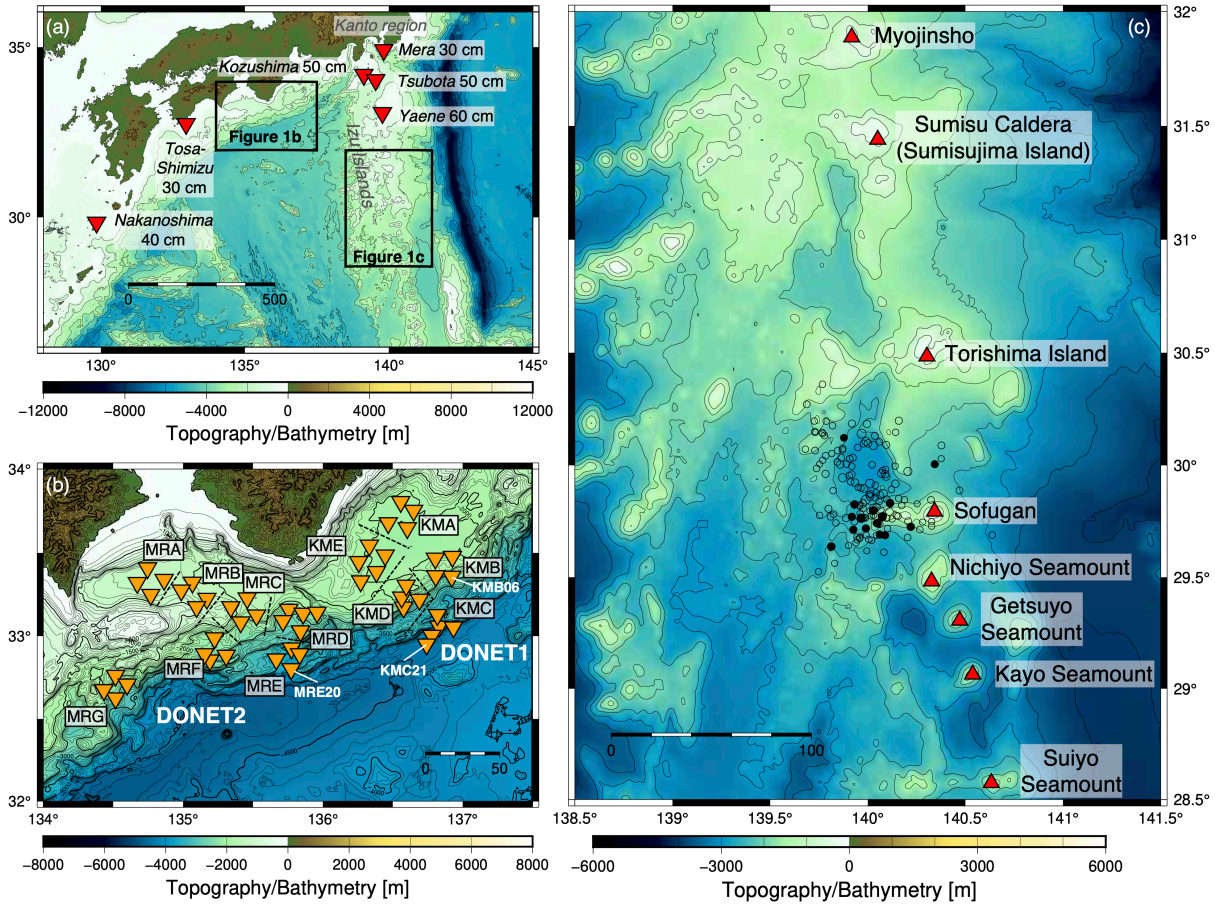

Figure 1. Maps of the study area. (**a**) Philippine Sea off southwestern Japan region. Red inverted triangles represent locations of tide gauges with maximum tsunami heights reported by JMA. (**b**) Orange inverted triangles represent the DONET stations; each DONET node (e.g., KMA, or MRA) contains 4 or 5 OBPs (each triangle). The tsunami is expected to arrive the earliest at KMC21 and MRE20 among DONET1 and DONET2, respectively. The OBS record at KMB06 is used for the T-phase analysis. (**c**) The region near Sofugan volcano. Circles represent the locations of seismic events at depths of <20 km from 1 to 8 October 2023, reported in the USGS earthquake catalog; open and closed circles indicate those before and after 18:00 on 8 October, respectively. Red triangles represent active volcanoes documented by Hydrographic and Oceanographic Department, Japan Coast Guard (2006).

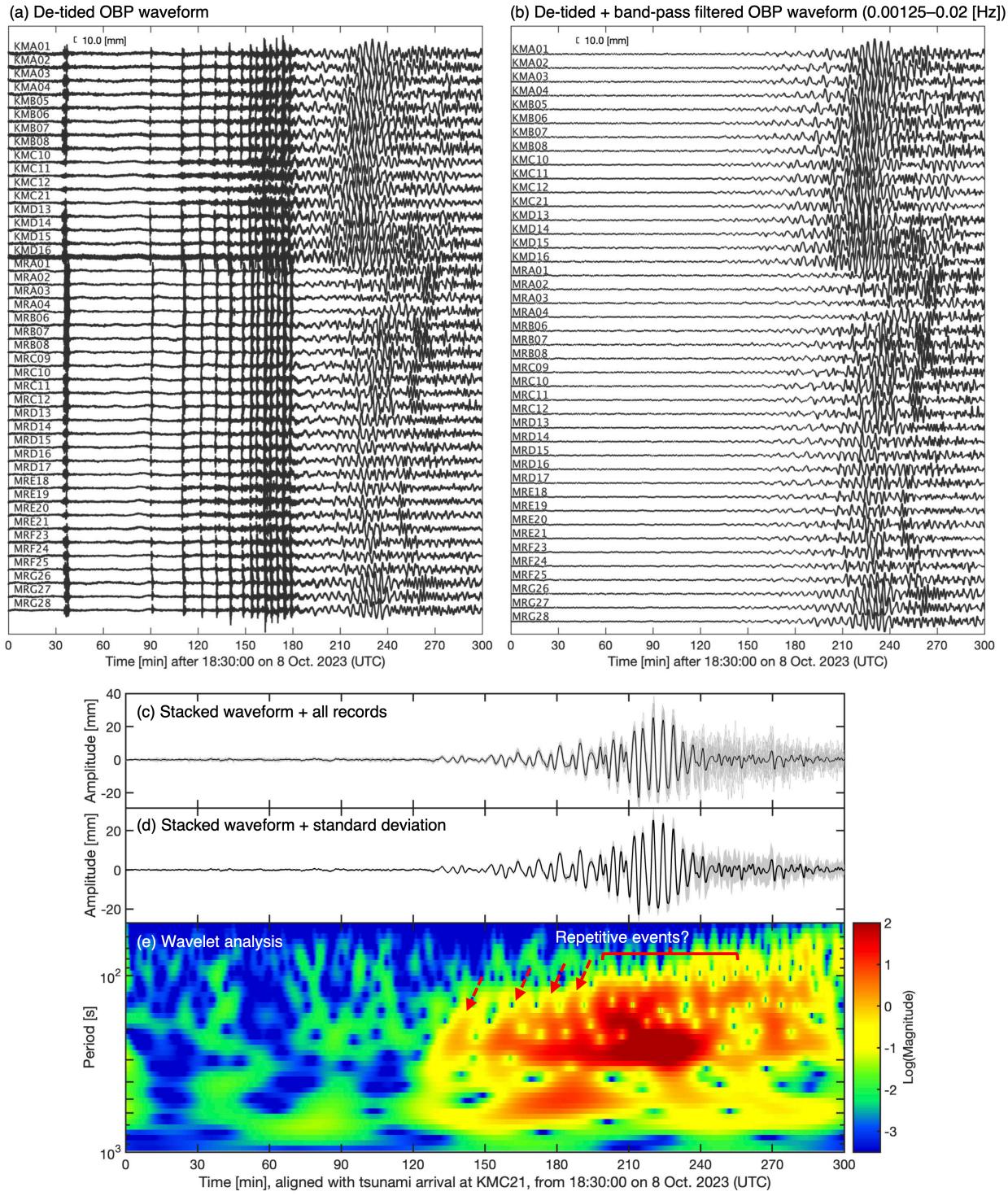

316

317 **Figure 2**. OBP waveforms recorded by DONET. (**a**) Waveforms after removing the tidal

318 component by polynomial approximation, and (**b**) after the tidal-component removal and the

band-pass filter (0.00125–0.02 Hz). The amplitudes are in unit of water wave height [mm] converted from pressure, using 1.0 [Pa] = 0.102 [mmH_2O]. (**c**) The stacked tsunami waveform (thick black line) and the 16 waveforms of DONET1 used for the stacking (thin gray line; Table S2). The time is aligned with the tsunami arrival at KMC21 (Figure 1b). (**d**) The stacked waveform (average amplitude; thick black line) ± standard deviation (shaded by gray). Wavelet analysis by the continuous wavelet transformation in MATLAB (Lilly, 2017). Red arrows and a bracket indicate multiple bands of amplitude peaks of tsunami wave trains.

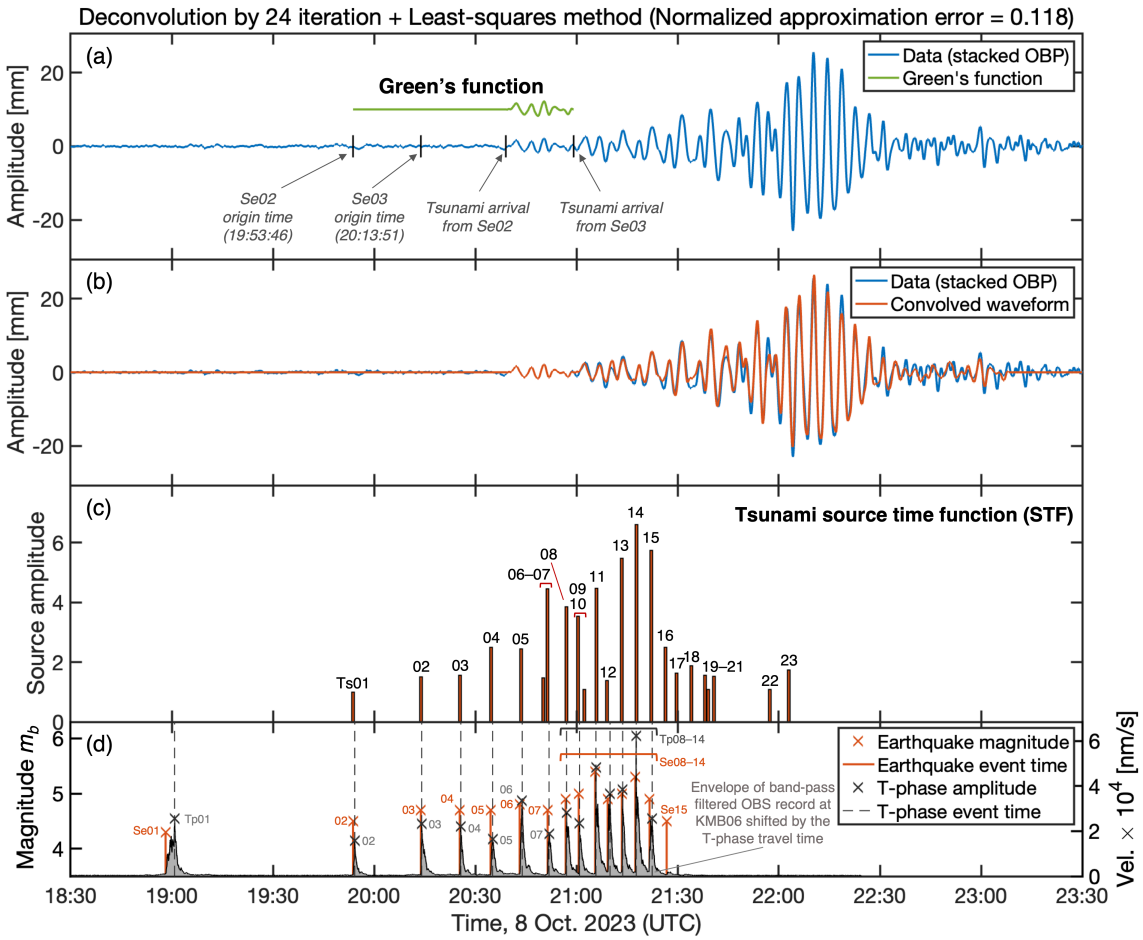

Figure 3. The tsunami STF by the 24 iterative deconvolutions and the least-squares method using DONET1. (**a**) The empirical Green's function (green line) obtained from the stacked tsunami waveform of (blue line). (**b**) The convolved tsunami waveform (red line) compared with the stacked waveform. (**c**) Tsunami STF, composed of 23 source events (Ts01–Ts23; Table S3). The source amplitudes are relative to that of Ts01. (**d**) The temporal history of the seismic (Se01–15) and T-phase events (Tp01–14), and the envelope of the vertical component of OBS at KMB06 (Figure 1b), shifted backward in time assuming the T-phase speed at 1.5 km/s (gray shade).

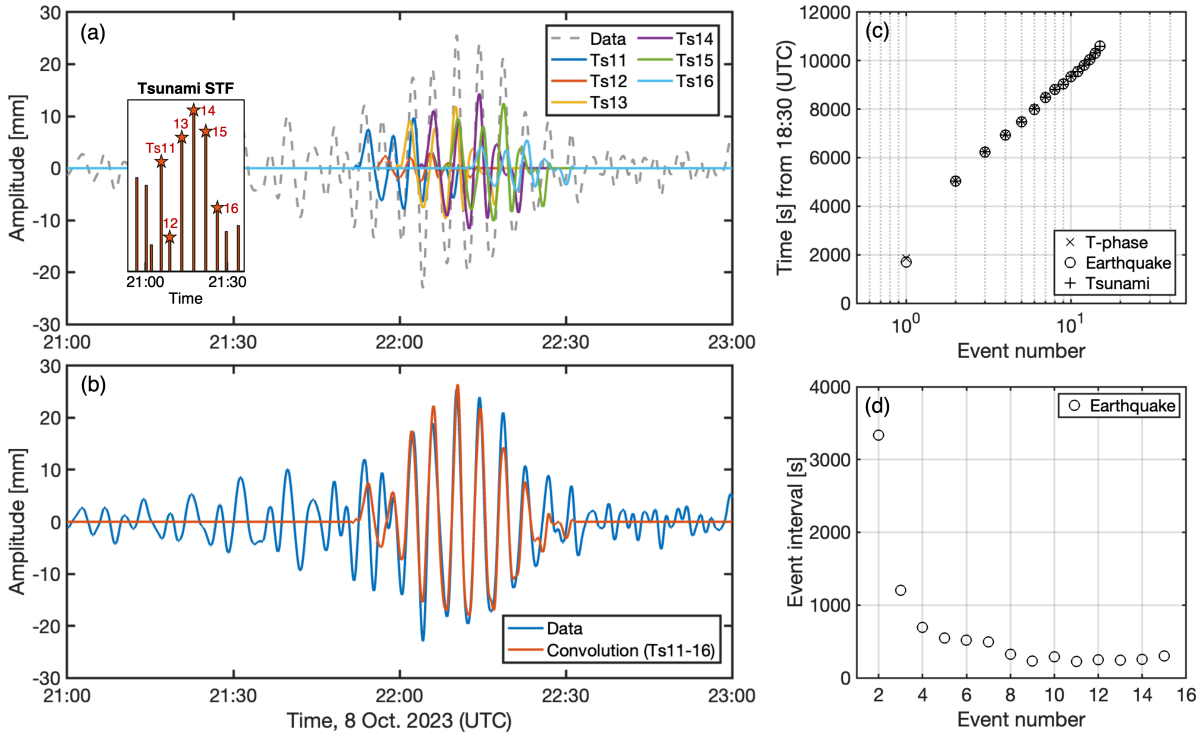

336

337 **Figure 4**. Tsunami waves of the later events. (**a**) The waveforms due to each of Ts11–16, shown
338 in the inset panel. (**b**) The convolved waveform with Ts11–16 (orange line) and the stacked
339 waveform of DONET1 (blue line). (**c**–**d**) The relationships between (**c**) the event number and
340 timing, determined by tsunamis, seismic waves, and/or T-phases, and (**d**) between the event
341 number and the inter-event times of the seismic events.

342

Acknowledgments

We thank Editor, Germán Prieto, and Associate Editor, Victor Tsai, for handling our manuscript, and two anonymous reviewers for their constructive comments and suggestions. We thank Tatsuhiko Saito for helpful discussion. This work is funded by the Sasakawa Scientific Research Grant from the Japan Science Society (Grant number 2023–2031).

Open Research

DONET data is available from NIED (National Research Institute for Earth Science and Disaster Resilience, 2019) (https://www.seafloor.bosai.go.jp/). We use bathymetric data of JTOPO30, which are available from Japan Hydrographic Association (https://www.jha.or.jp/shop/index.php?main_page=advanced_search_result&categories_id=1302) (http://www.mirc.jha.jp/products/finished/JTOPO30/). Earthquake information is available from U. S. Geological Survey (USGS: https://earthquake.usgs.gov/earthquakes/search/, accessed on 21 December 2023).

References

Abe, K. (1981). Physical size of tsunamigenic earthquakes of the northwestern Pacific. *Physics of the Earth and Planetary Interiors*, *27*(3), 194–205. https://doi.org/10.1016/0031-9201(81)90016-9

Earthquake Research Institute, The University of Tokyo. (2023, November 9). Analysis: Chemical compositions of drifting pumice collected near Izu-Torishima and Sofugan Islands rock (in Japanese). Retrieved December 25, 2023, from https://www.eri.u-tokyo.ac.jp/eq/20272/

Ewing, M., Tolstoy, I., & Frank Press. (1950). Proposed use of the T phase in tsunami warning systems. *Bulletin of the Seismological Society of America*, *40*(1), 53–58. https://doi.org/10.1785/BSSA0400010053

Fukao, Y., Sandanbata, O., Sugioka, H., Ito, A., Shiobara, H., Watada, S., & Satake, K. (2018). Mechanism of the 2015 volcanic tsunami earthquake near Torishima, Japan. *Science Advances*, *4*(4), eaao0219. https://doi.org/10.1126/sciadv.aao0219

Geological Survey of Japan, National Institute of Advanced Industrial Science and Technology (2023). Characteristics of drifted pumice collected near Torishima Island in October 2023 (in Japanese). Retrieved December 25, 2023, from https://www.gsj.jp/hazards/volcano/torishima/index.html

Global Volcanism Program. (2023). Sofugan (284091). In E. Venzke (Ed.), *Volcanoes of the World (v. 5.1.5; 15 Dec 2023)*. Smithsonian Institution. Retrieved from https://volcano.si.edu/volcano.cfm?vn=284091

Grilli, S. T., Tappin, D. R., Carey, S., Watt, S. F. L., Ward, S. N., Grilli, A. R., et al. (2019). Modelling of the tsunami from the December 22, 2018 lateral collapse of Anak Krakatau volcano in the Sunda Straits, Indonesia. *Scientific Reports*, *9*(1), 11946. https://doi.org/10.1038/s41598-019-48327-6

Hotovec, A. J., Prejean, S. G., Vidale, J. E., & Gomberg, J. (2013). Strongly gliding harmonic tremor during the 2009 eruption of Redoubt Volcano. *Journal of Volcanology and Geothermal Research*, *259*, 89–99. https://doi.org/10.1016/j.jvolgeores.2012.01.001

Hydrographic and Oceanographic Department, Japan Coast Guard. (2006). Database of the Maritime and Submarine Volcanoes in Japan. Retrieved October 14, 2023, from https://www1.kaiho.mlit.go.jp/kaiikiDB/list-2.htm

Igarashi, G. (2000). A geodetic sign of the critical point of stress‐strain state at a plate boundary. *Geophysical Research Letters*, *27*(13), 1973–1976. https://doi.org/10.1029/1999gl005443

Japan Coast Guard (2023). Report on drifted material in the sea around Torishima Island (observed on October 20) (in Japanese). Retrieved December 25, 2023, from https://www.kaiho.mlit.go.jp/info/kouhou/post-1041.html

Japan Agency for Marine-Earth Science and Technology. (2023). Emergency Research cruise by the submarine research vessel "KAIMEI" in the sea around Torishima Island (Prompt Report) (in Japanese). Retrieved December 25, 2023, from https://www.jamstec.go.jp/j/about/press_release/20231121/

Japan Meteorological Agency. (2013). Sofugan. In *NATIONAL CATALOGUE OT THE ACTIVE VOLCANOES IN JAPAN (THE FORTH EDITION)*. Retrieved from https://www.data.jma.go.jp/vois/data/tokyo/STOCK/souran_eng/volcanoes/069_sofugan.pdf

Japan Meteorological Agency. (2023, October 9). Report on Earthquake near Torishima Island around 5:25 on October 9, 2023 (2nd report) (in Japanese). Retrieved October 19, 2023, from https://www.jma.go.jp/jma/press/2310/09b/202310091100.html

Kanamori, H. (1972). Mechanism of tsunami earthquakes. *Physics of the Earth and Planetary Interiors*, *6*(5), 346–359. https://doi.org/10.1016/0031-9201(72)90058-1

Kanamori, H., Ekström, G., Dziewonski, A., Barker, J. S., & Sipkin, S. A. (1993). Seismic radiation by magma injection: An anomalous seismic event near Tori Shima, Japan. *Journal of Geophysical Research*, *98*(B4), 6511–6522. https://doi.org/10.1029/92jb02867

Kikuchi, B. Y. M., & Kanamori, H. (1982). Inversion of complex body waves. *Bulletin of the Selsmologmal Socmty of America*, *72*(2), 491–506. X

Kodaira, S., Sato, T., Takahashi, N., Ito, A., Tamura, Y., Tatsumi, Y., & Kaneda, Y. (2007). Seismological evidence for variable growth of crust along the Izu intraoceanic arc. *Journal of Geophysical Research*, *112*(B5), B05104. https://doi.org/10.1029/2006jb004593

Kubota, T., Saito, T., & Nishida, K. (2022). Global fast-traveling tsunamis driven by atmospheric Lamb waves on the 2022 Tonga eruption. *Science*, *377*(6601), 91–94. https://doi.org/10.1126/science.abo4364

Lawson, C. L., & Hanson, R. J. (1974). Chapter 23. Linear Least Squares with Linear Inequality Constraints. In *Solving Least-Squares Problems* (p. 161). Upper Saddle River, NJ: Prentice Hall.

Lilly, J. M. (2017). Element analysis: a wavelet-based method for analysing time-localized events in noisy time series. *Proceedings. Mathematical, Physical, and Engineering Sciences / the Royal Society*, *473*(2200), 20160776. https://doi.org/10.1098/rspa.2016.0776

Maeno, F., Imamura, F., & Taniguchi, H. (2006). Numerical simulation of tsunamis generated by caldera collapse during the 7.3 ka Kikai eruption, Kyushu, Japan. *Earth, Planets and Space*, *58*(8), 1013–1024. https://doi.org/10.1186/BF03352606

Matsumoto, H., Haralabus, G., Zampolli, M., & Özel, N. M. (2016). T‐phase and tsunami pressure waveforms recorded by near‐source IMS water‐column hydrophone triplets during the 2015 Chile earthquake. *Geophysical Research Letters*, *43*(24). https://doi.org/10.1002/2016gl071425

Michon, L., Villeneuve, N., Catry, T., & Merle, O. (2009). How summit calderas collapse on basaltic volcanoes: New insights from the April 2007 caldera collapse of Piton de la Fournaise volcano. *Journal of Volcanology and Geothermal Research*, *184*(1), 138–151. https://doi.org/10.1016/j.jvolgeores.2008.11.003

Mizutani, A., & Melgar, D. (2023). Potential volcanic origin of the 2023 short-period tsunami in the Izu Islands, Japan. *Seismica*, *2*(2). https://doi.org/10.26443/seismica.v2i2.1160

Mulia, I. E., Watada, S., Ho, T.-C., Satake, K., Wang, Y., & Aditiya, A. (2020). Simulation of the 2018 tsunami due to the flank failure of anak krakatau volcano and implication for future observing systems. *Geophysical Research Letters*, *47*(14), e2020GL087334. https://doi.org/10.1029/2020gl087334

National Research Institute for Earth Science and Disaster Resilience. (2019). NIED DONET [Data set]. National Research Institute for Earth Science and Disaster Resilience. https://doi.org/10.17598/NIED.0008

Okal, E. A. (2003). T Waves from the 1998 Papua New Guinea Earthquake and its Aftershocks: Timing the Tsunamigenic Slump. In J.-P. Bardet, F. Imamura, C. E. Synolakis, E. A. Okal, & H. L. Davies (Eds.), *Landslide Tsunamis: Recent Findings and Research Directions* (pp. 1843–1863). Basel: Birkhäuser Basel. https://doi.org/10.1007/978-3-0348-7995-8_4

Okal, E. A. (2008). The generation of T waves by earthquakes. In R. Dmowska (Ed.), *Advances in Geophysics* (Vol. 49, pp. 1–65). Elsevier. https://doi.org/10.1016/S0065-2687(07)49001-X

Paris, R. (2015). Source mechanisms of volcanic tsunamis. *Philosophical Transactions. Series A, Mathematical, Physical, and Engineering Sciences*, *373*(2053). https://doi.org/10.1098/rsta.2014.0380

Purkis, S. J., Ward, S. N., Fitzpatrick, N. M., Garvin, J. B., Slayback, D., Cronin, S. J., et al. (2023). The 2022 Hunga-Tonga megatsunami: Near-field simulation of a once-in-a-century event. *Science Advances*, *9*(15), eadf5493. https://doi.org/10.1126/sciadv.adf5493

Sandanbata, O., Kanamori, H., Rivera, L., Zhan, Z., Watada, S., & Satake, K. (2021). Moment tensors of ring-faulting at active volcanoes: Insights into vertical-CLVD earthquakes at the Sierra Negra caldera, Galápagos islands. *Journal of Geophysical Research, [Solid Earth]*, *126*(6), e2021JB021693. https://doi.org/10.1029/2021jb021693

Sandanbata, O., & Saito, T. (2024). Quantifying Magma Overpressure Beneath a Submarine Caldera: A Mechanical Modeling Approach to Tsunamigenic Trapdoor Faulting Near Kita-Ioto Island, Japan. *Journal of Geophysical Research, [Solid Earth]*, *129*(1), e2023JB027917. https://doi.org/10.1029/2023JB027917

Sandanbata, O., Watada, S., Satake, K., Kanamori, H., Rivera, L., & Zhan, Z. (2022). Sub‐decadal volcanic tsunamis due to submarine trapdoor faulting at sumisu caldera in the Izu–Bonin arc. *Journal of Geophysical Research, [Solid Earth]*, *127*(9), e2022JB024213. https://doi.org/10.1029/2022jb024213

Sandanbata, O., Watada, S., Satake, K., Kanamori, H., & Rivera, L. (2023). Two volcanic tsunami events caused by trapdoor faulting at a submerged caldera near Curtis and Cheeseman islands in the kermadec arc. *Geophysical Research Letters*, *50*(7), e2022GL101086. https://doi.org/10.1029/2022gl101086

476 Satake, K., & Kanamori, H. (1991). Abnormal tsunamis caused by the June 13, 1984, Torishima,
477 Japan, earthquake. *Journal of Geophysical Research*, *96*(B12), 19933–19939.
478 https://doi.org/10.1029/91jb01903
479 Sugioka, H., Fukao, Y., Kanazawa, T., & Kanjo, K. (2000). Volcanic events associated with an
480 enigmatic submarine earthquake. *Geophysical Journal International*, *142*(2), 361–370.
481 https://doi.org/10.1046/j.1365-246x.2000.00153.x
482 Synolakis, C. E., Bardet, J.-P., Borrero, J. C., Davies, H. L., Okal, E. A., Silver, E. A., et al.
483 (2002). The slump origin of the 1998 Papua New Guinea Tsunami. *Proceedings of the*
484 *Royal Society of London. Series A: Mathematical, Physical and Engineering Sciences*,
485 *458*(2020), 763–789. https://doi.org/10.1098/rspa.2001.0915
486 Tanioka, Y., & Satake, K. (1996). Fault parameters of the 1896 Sanriku Tsunami Earthquake
487 estimated from Tsunami Numerical Modeling. *Geophysical Research Letters*, *23*(13),
488 1549–1552. https://doi.org/10.1029/96GL01479
489 Tappin, D. R., Matsumoto, T., Watts, P., Satake, K., McMurtry, G. M., Matsuyama, M., et al.
490 (1999). Sediment slump likely caused 1998 Papua New Guinea tsunami. *Eos*, *80*(30),
491 329. https://doi.org/10.1029/99eo00241
492 Wang, T. A., Segall, P., Hotovec-Ellis, A. J., Anderson, K. R., & Cervelli, P. F. (2023). Ring
493 fault creep drives volcano-tectonic seismicity during caldera collapse of Kīlauea in 2018.
494 *Earth and Planetary Science Letters*, *618*, 118288.
495 https://doi.org/10.1016/j.epsl.2023.118288
496 Wang, Y., Heidarzadeh, M., Satake, K., & Hu, G. (2022). Characteristics of two tsunamis
497 generated by successive M_w 7.4 and M_w 8.1 earthquakes in the Kermadec Islands on 4

March 2021. *Natural Hazards and Earth System Sciences*, *22*(3), 1073–1082. https://doi.org/10.5194/nhess-22-1073-2022

Wech, A., Tepp, G., Lyons, J., & Haney, M. (2018). Using earthquakes, *T* waves, and infrasound to investigate the eruption of Bogoslof volcano, Alaska. *Geophysical Research Letters*, *45*(14), 6918–6925. https://doi.org/10.1029/2018gl078457

Yamada, M., Mori, J., & Matsushi, Y. (2016). Possible stick‐slip behavior before the Rausu landslide inferred from repeating seismic events. *Geophysical Research Letters*, *43*(17), 9038–9044. https://doi.org/10.1002/2016gl069288

Yamasato, H., Hamada, N., McCreery, C. S., Oliveira, F. J., Walker, D. A., & Talandier, J. (1993). T Waves Associated with Submarine Volcanic Eruptions in the Marianas Observed by Ocean Bottom Seismographs. *Journal of Physics of the Earth*, *41*(2), 57–74.https://doi.org/10.4294/jpe1952.41.57